Unlocking Mo, P co-doping to boost proton intercalation in MnO_2 as a high-performance cathode material for aqueous zinc-ion batteries

Kaixuan Ma[a, d], Guangfeng Liang[a], Qingze Jiao[a, b], Haibo Jin[b, c], Yuefeng Su[b, c], Ning Li[b, c], Jingbo Li[b, c], Zhiyong Xiong[b], Caihong Feng[a, b*], Yun Zhao[a*]

a Beijing Key Laboratory for Chemical Power Source and Green Catalysis, School of Chemistry and Chemical Engineering, Beijing Institute of Technology, Beijing 100081, People's Republic of China

b Beijing Institute of Technology (Zhuhai Campus), Zhuhai 519088, China

c School of Materials Science and Engineering Beijing Key Laboratory of Environmental Science and Engineering Beijing Institute of Technology Beijing 100081 P. R. China

d BAIC Foton Automotive Co., Ltd, Beijing 102206, China

*Corresponding authors. E-mail address

Caihong Feng, E-mail: fengch@bit.edu.cn

Yun Zhao, E-mail: Zhaoyun@bit.edu.cn

S1. Experimental

Experimental methods

Synthesis of Mo doping MnO_2 nanoflowers

0.056 g of $MnSO_4·4H_2O$ and 0.32 g of $KMnO_4$ were dissolved in 48 mL of deionized water and stirred for 5 minutes. Then 0.0 g (noted as MnO_2) or 0.024 g ($MnSO_4·4H_2O$ to $(NH_4)_6Mo_7O_{24}·4H_2O$ was 1:0.06, noted as Mo-MnO_2) of $(NH_4)_6Mo_7O_{24}·4H_2O$ was added to the mixed solution and stirred for 5 minutes. Transfer the above solution to a polytetrafluoroethylene autoclave heat to 160 °C and hold for 12 hours. Subsequently, samples were collected by centrifugation and washed several times with deionized water. Finally, Samples were dried under vacuum at 60 °C.

Synthesis of Mo, P co-doping MnO_2 nanoflowers

For Mo, P co-doped MnO_2 (Mo, P-MnO_2), NaH_2PO_2 (the mass ratio of Mo-MnO_2 to NaH_2PO_2 was 1:0.7) was placed upstream and prepared Mo-MnO_2 was placed downstream and heated up to 300 °C at 2 °C min^{-1} and kept for 60 min. P-doped MnO_2 (P-MnO_2) was prepared as described above, with NaH_2PO_2 upstream and prepared MnO_2 downstream. All the processes were carried out under argon atmosphere.

Material characterization

The crystallinity of the samples was examined by the powder X-ray diffraction

(XRD, Bruker, Germany) with Cu Kα at 40 kV at the 2θ range from 5° to 80°. The morphologies and structures of samples were characterized by scanning electron microscope (SEM, JSM-7500F), transmission electron microscopy (TEM, Hitachi HT7700), high-resolution transmission electron microscopy (HRTEM, Hitachi HT7700), and high-angle annular dark-field scanning transmission electron microscopy (HAADF-STEM). Surface valence states of samples were tested by X-ray photoelectron spectroscopy (XPS, ESCALAB 250Xi). Deionized water was used to test the hydrophilicity of samples via contact angle instruments (OCA-20, DataPhysics, Germany).

Electrochemical measurements

The electrochemical properties of the samples were evaluated by assembling CR2025 coin cells. Mo, P-MnO_2, conductive additive (Super P), and polyvinylidene fluoride (PVDF) were ground evenly at a weight ratio of 7:2:1, and then N-methyl pyrrolidone (NMP) was added to form the slurry. The slurry was coated on stainless steel mesh and dried at 80 °C to prepare cathode material. Besides, Zinc foil, glass fiber, and 2.0 M $ZnSO_4$ + 0.2 M $MnSO_4$ were used as anodes, diaphragms, and electrolytes, respectively.

The sandwich-like flexible ZIBs were assembled by using Zn foil, polyacrylamide (PAM) hydrogel, and Mo, P-MnO_2 as anode, electrolyte, and cathode, respectively, and then sealed by polyimide (PI) film. The PAM hydrogel electrolyte with a thickness of ~ 0.4 mm was prepared in a typical way [1]. Preparation of the PAM hydrogel electrolyte

included several steps. Firstly, 1 g of acrylamide monomer was dissolved in 3 ml deionized water, and then 1 mg of N, N'- methylenebisacrylamide crosslinker was introduced and stirred for 10 min. Subsequently, 16 mg of APS was added to initiate the crosslinking reaction. After a continuous magnetic stirring for 5 min, the above mixture was poured into a glass mold and maintained at 65 ◦C for 1 h to form a PAM hydrogel film. Finally, the PAM hydrogel film was soaked in a 2 M $ZnSO_4$/0.1 $MnSO_4$ mixture solution for 24 h to get a film-like PAM hydrogel electrolyte with a thickness of ~ 0.3 mm.

Cyclic voltammetry (CV) was performed at a potential window of 0.8–1.8 V on an electrochemical workstation (CHI660D). Electrochemical impedance spectroscopy (EIS) was also tested at CHI660D at frequencies from 0.01 Hz to 100 kHz. The galvanostatic discharge/charge test and the galvanostatic intermittence titration technique (GITT) were studied using a multichannel battery testing system (LAND, CT2001A).

Computational details

DFT implemented in Vienna Ab initio simulation package (VASP) is used in all calculations. The exchange correlation potential is described by the generalized gradient approximation of Perdew-Burke-Ernzerhof (GGA-PBE). The interaction between ion core and valence electron is treated by projection enhanced wave (PAW) method. The cutoff energy of plane wave is fixed at 450 eV. Relax the given structural model until the Hellmann-Feynman force is less than -0.02eV and the energy change is

less than 10^{-6} eV. Grimme's DFT-D3 method is used to describe the dispersed interactions between all atoms in the adsorption model.

Relevant calculation equations

To explore the dynamics in the cell, the peak current (i) and scan rate (v) are related by the following equation:

$$i = av^b \quad \text{(S1)}$$

where a and b are parameters to be determined. The electrochemical charge storage mechanism is characterized by the value of b, which is in the range of 0.5 to 1, with values close to 0.5 indicating diffusion-controlled reactions and close to 1 indicating capacitive processes.

The capacitive and diffusive contribution ratios of MnO_2 and Mo, P-MnO_2 can be quantitatively calculated based on the following equation:

$$i = k_1v + k_2v^{1/2} \quad \text{(S2)}$$

The capacitive effect and the diffusion control process are represented by the values of k_1v and $k_2v^{1/2}$, respectively.

Ion transport kinetics are further evaluated by GITT technique. The calculation formula is as follows:

$$D_{ion} = (4/\pi\tau)\,(m_A V_M/M_A S)^2(\Delta E_s/\Delta E_\tau)^2 \quad \text{(S3)}$$

where m_A (g), V_M ($cm^3\ mol^{-1}$), and M_A ($g\ mol^{-1}$) are the mass, molar volume, and molecular weight of the cathode, respectively. τ is the relaxation time (s), s is the electrode area (cm^2), ΔEt is the voltage change (V) during the current pulse, and ΔEs is

the steady state potential change (V).

S2. Supporting Figures

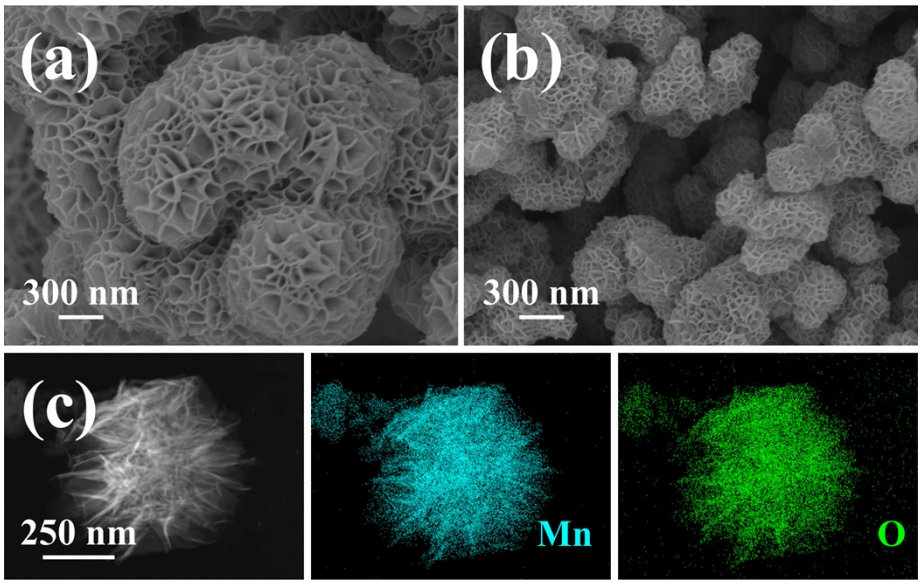

Fig.S1. SEM images of (a) P-MnO_2, (b) Mo-MnO_2. (c) HAADF-STEM and corresponding elemental mapping images for Mn and O elements of the MnO_2.

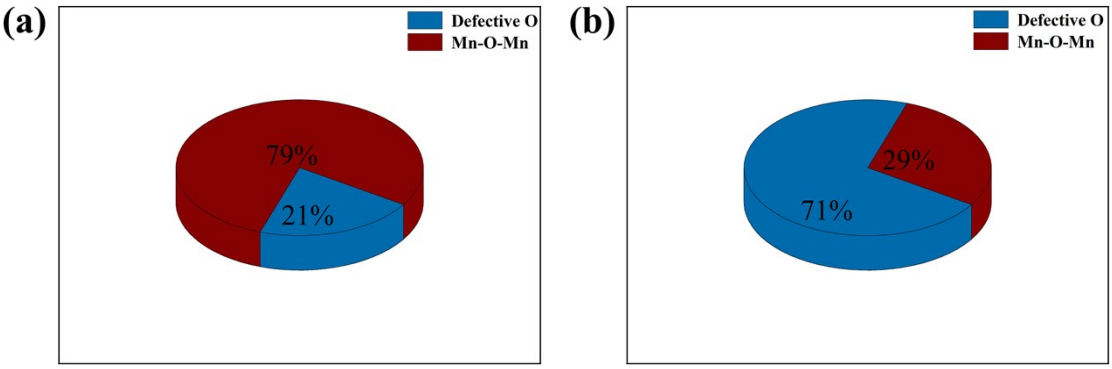

Fig.S2. The ratio of defective O to Mn-O-Mn in (a) MnO_2 and (b) Mo, P-MnO_2.

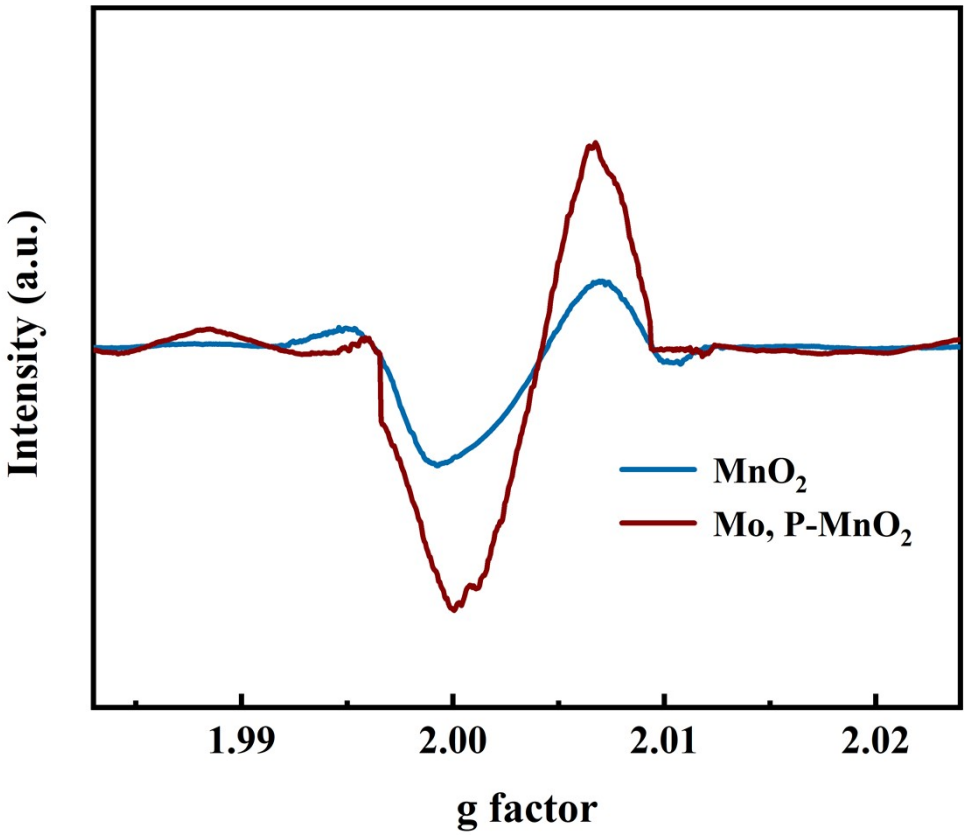

Fig.S3. EPR of MnO_2 and Mo, P-MnO_2.

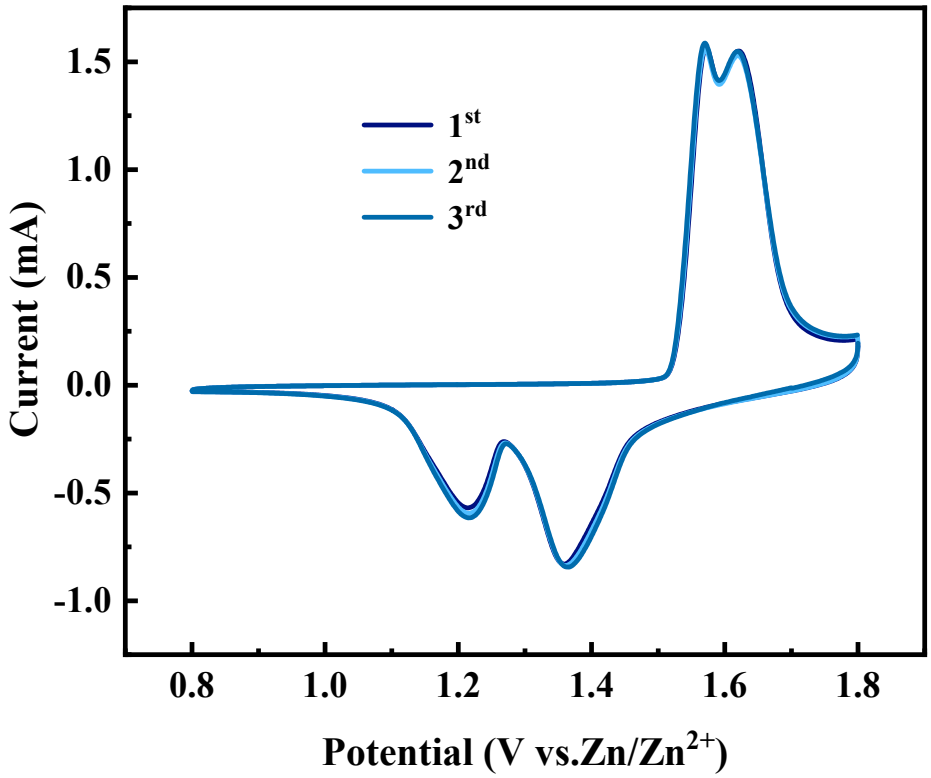

Fig.S4. CV curves of Mo, P-MnO_2 in the initial three cycles.

Table S1. Rate performance of MnO_2, Mo-MnO_2, P-MnO_2, and Mo, P-MnO_2 at various currents.

	MnO_2	Mo-MnO_2	P-MnO_2	Mo, P-MnO_2
0.1 A g^{-1}	257.5 mAh g^{-1}	353.2 mAh g^{-1}	267.3 mAh g^{-1}	367.6 mAh g^{-1}
0.3 A g^{-1}	185.0 mAh g^{-1}	303.1 mAh g^{-1}	266.5 mAh g^{-1}	356.8 mAh g^{-1}
0.5 A g^{-1}	143.9 mAh g^{-1}	236.1 mAh g^{-1}	257.6 mAh g^{-1}	332.7 mAh g^{-1}
1 A g^{-1}	115.3 mAh g^{-1}	188.6 mAh g^{-1}	226.3 mAh g^{-1}	289.7 mAh g^{-1}
2 A g^{-1}	94.6 mAh g^{-1}	157.3 mAh g^{-1}	192.2 mAh g^{-1}	240.6 mAh g^{-1}
3 A g^{-1}	88.3 mAh g^{-1}	125.1 mAh g^{-1}	162.2 mAh g^{-1}	202.0 mAh g^{-1}
5 A g^{-1}	75.0 mAh g^{-1}	85.8 mAh g^{-1}	110.8 mAh g^{-1}	146.6 mAh g^{-1}

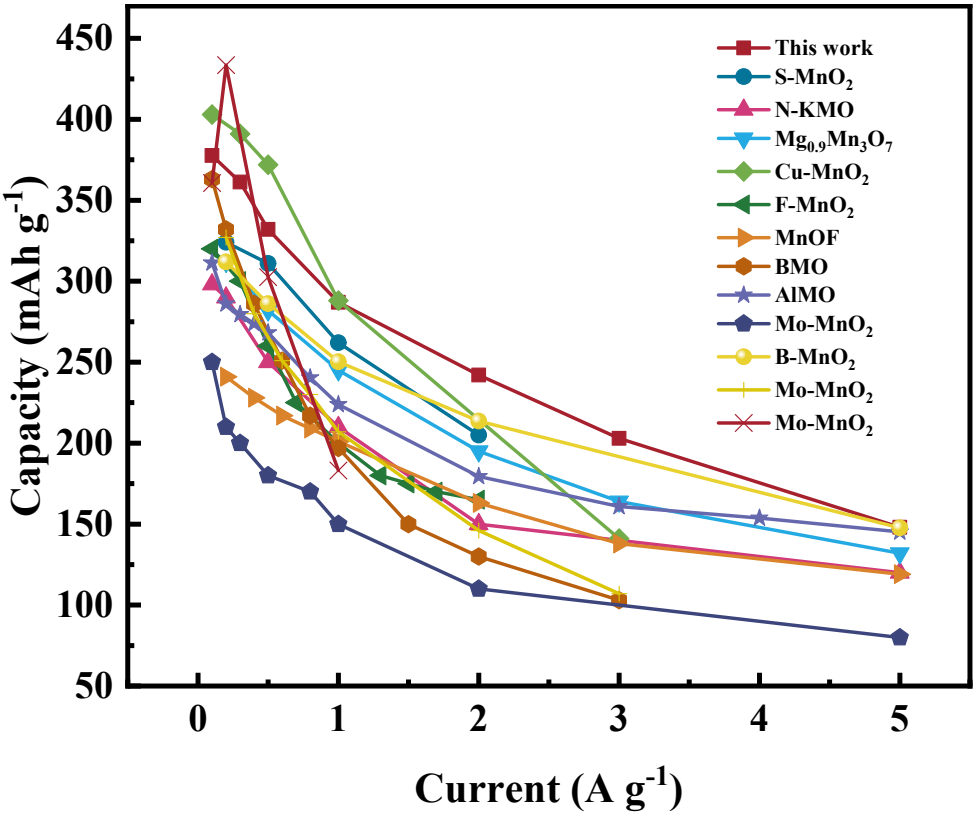

Fig.S5. Comparison of rate performance of Mo, P-MnO_2 with some previous manganese-based cathodes for ZIBs. [2-13]

The cells are first activated at a low current density of 0.1 A g^{-1} for 20 cycles and then cycle at 0.3 A g^{-1} (inset in **Fig. S6(a)** and **Fig. S6(b)**) or 1.0 A g^{-1} (inset in **Fig. S7(a)** and **Fig. S7(b)**). The capacities of MnO_2 and Mo, P-MnO_2 all exhibit an upward trend at 0.1 A g^{-1} during the activation process. When the electrode discharges at a small current density, the electrochemical polarization is relatively small, which means that the charge distribution on the electrode surface is relatively uniform and the active material can be fully utilized. Therefore, the capacity of the electrode will increase at a small current density (0.1 A g^{-1} or 0.3 A g^{-1}). The gradual increase in capacity with the increase of cycles is also common in other transition metal oxides, including FeO_x and Mn-based materials[14, 15]. The possible reasons in this case can be attributed to gradual penetration of electrolyte [16-18], slow reversible reactions of the active materials[2, 19-21], and in situ electrochemical activation[22-24].

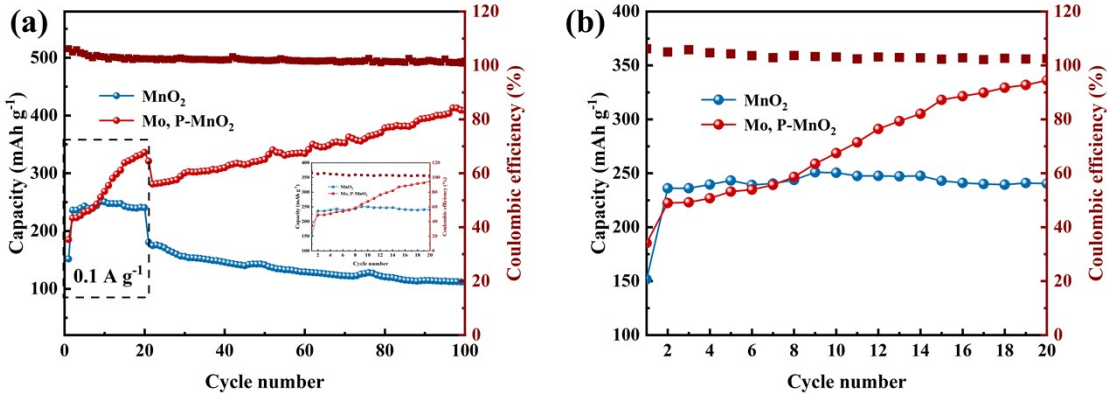

Fig.S6. (a) Cycling performance of MnO_2 and Mo, P-MnO_2 at 0.3 A g^{-1} (Inset in (a) shows the corresponding activation process at 0.1 A g^{-1} over 20 cycles). (b) the corresponding activation process at 0.1 A g^{-1} over 20 cycles.

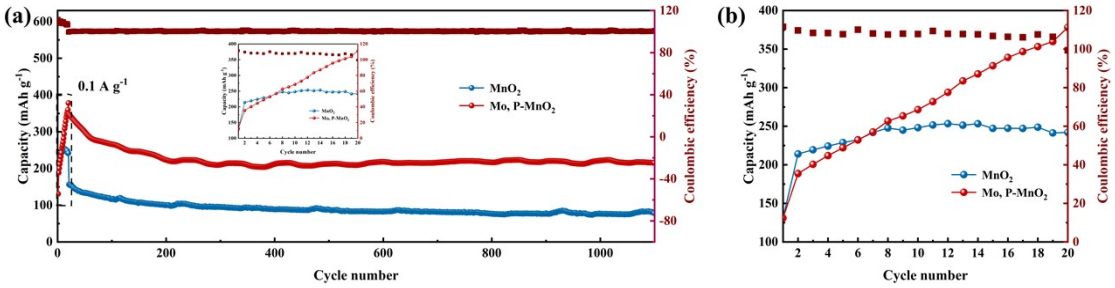

Fig.S7. (a) Cycling performance of MnO_2 and Mo, P-MnO_2 at 1.0 A g^{-1} (Inset in (a) shows the corresponding activation process at 0.1 A g^{-1} over 20 cycles). (b) the corresponding activation process at 0.1 A g^{-1} over 20 cycles.

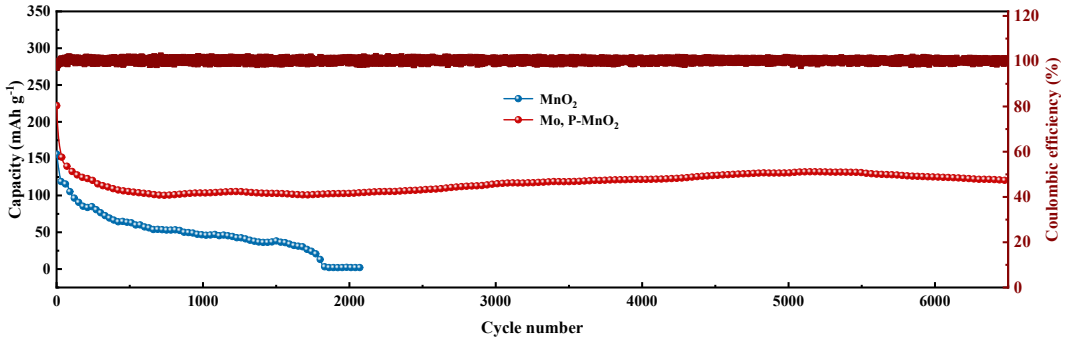

Fig.S8. Cycling performance of MnO_2 and Mo, P-MnO_2 at 1.5 A g^{-1}.

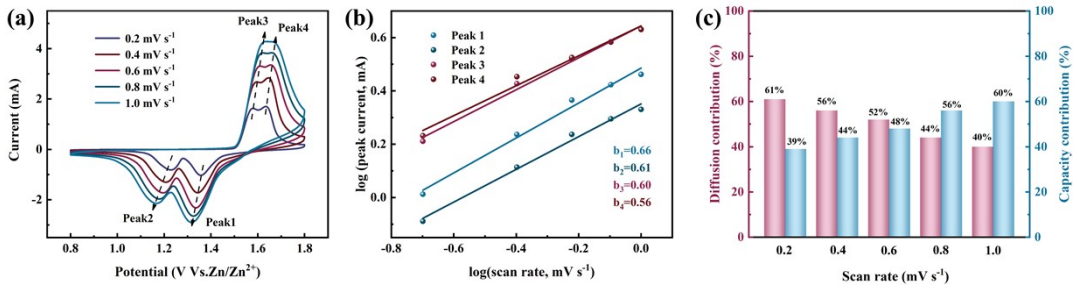

Fig.S9. (a) CV curves of MnO_2 at various current densities (b) linear fitting profiles of log (i) ~log (v). (c) Various contribution ratios of capacitance at different scanning rates in the MnO_2 electrode.

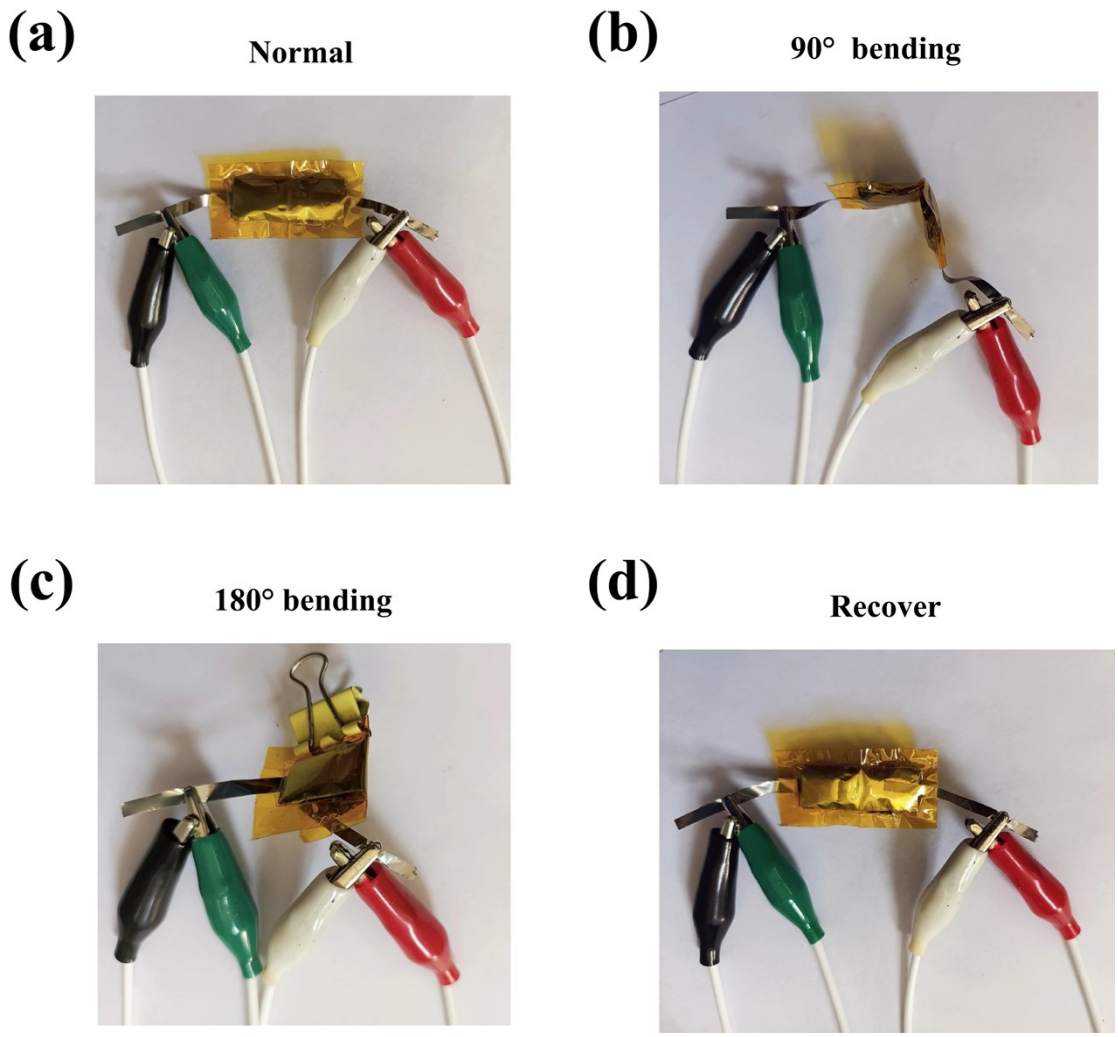

Fig.S10. Photos of Mo, P-MnO_2 flexible ZIB under different bending states.

References

1. Y. Li, X. Li, H. Duan, S. Xie, R. Dai, J. Rong, F. Kang and L. Dong, *Chemical Engineering Journal*, 2022, **441**, 136008.

2. Y. Zhao, P. Zhang, J. Liang, X. Xia, L. Ren, L. Song, W. Liu and X. Sun, *Energy Storage Materials*, 2022, **47**, 424-433.

3. G. Cui, Y. Zeng, J. Wu, Y. Guo, X. Gu and X. W. D. Lou, *Advanced Science*, 2022, **9**, 1-9.

4. J. Li, N. Luo, L. Kang, F. Zhao, Y. Jiao, T. J. Macdonald, M. Wang, I. P. Parkin, P. R. Shearing, D. J. L. Brett, G. Chai and G. He, *Advanced Energy Materials*, 2022, **12**, 202201840.

5. J. Zhang, W. Li, J. Wang, X. Pu, G. Zhang, S. Wang, N. Wang and X. Li, *Angewandte Chemie International Edition*, 2022, **62**, e202215654.

6. S. Kim, B.-R. Koo, Y.-R. Jo, H.-R. An, Y.-G. Lee, C. Huang and G.-H. An, *Journal of Materials Chemistry A*, 2021, **9**, 17211-17222.

7. L. Ding, L. Wang, J. Gao, T. Yan, H. Li, J. Mao, F. Song, S. Fedotov, L. Y. Chang, N. Li, Y. Su, T. Liu and L. Zhang, *Advanced Functional Materials*, 2023, **33**, 2301648.

8. Y. Ma, M. Xu, R. Liu, H. Xiao, Y. Liu, X. Wang, Y. Huang and G. Yuan, *Energy Storage Materials*, 2022, **48**, 212-222.

9. K. Wang, J. Wang, P. Chen, M. Qin, C. Yang, W. Zhang, Z. Zhang, Y. Zhen, F. Fu and B. Xu, *Small*, 2023, **19**, 2300585

10. Z. Zheng, G. Yang, J. Yao, J. Li, J. Zheng, Z. Wu, Y. Gan, C. Wang, L. Lv, H. Wan, C. Chen, H. Wang, L. Tao, J. Zhang and H. Wang, *Applied Surface Science*, 2022, **592**, 153335.

11. S. Deng, B. Xu, X. Liu, C.-W. Kan and T. Chen, *Chemical Engineering Journal*, 2023, **475**, 146098.

12. Z. Wang, K. Han, Q. Wan, Y. Fang, X. Qu and P. Li, *ACS Appl Mater Interfaces*, 2023, **15**, 859-869.

13. X. Xia, Y. Zhao, Y. Zhao, M. Xu, W. Liu and X. Sun, *Nano Research*, 2022, **16**, 2511-2518.

14. C. Zhu, G. Fang, J. Zhou, J. Guo, Z. Wang, C. Wang, J. Li, Y. Tang and S. Liang, *Journal of Materials Chemistry A*, 2018, **6**, 9677-9683.

15. X. Qi, H.-B. Zhang, J. Xu, X. Wu, D. Yang, J. Qu and Z.-Z. Yu, *ACS Applied Materials & Interfaces*, 2017, **9**, 11025-11034.

16. B. Wu, G. Zhang, M. Yan, T. Xiong, P. He, L. He, X. Xu and L. Mai, *Small*, 2018, **14**, 1703850.

17. Z. Li, Y. Zheng, Q. Jiao, Y. Zhao, H. Li and C. Feng, *Chemical Engineering Journal*, 2023, **465**, 142897.

18. Q. Wang, G. Tian, C. Huang and D. Zhang, *Small*, 2023, **19**, 2301189.

19. W. Jiang, X. Xu, Y. Liu, L. Tan, F. Zhou, Z. Xu and R. Hu, *Journal of Alloys and Compounds*, 2020, **827**, 154273.

20. W. Jiang, W. Wang, H. Shi, R. Hu, J. Hong, Y. Tong, J. Ma, C. jing Liang, J. Peng and Z. Xu, *Journal of Colloid and Interface Science*, 2023, **647**, 124-133.

21. W. Jiang, H. Shi, X. Xu, J. Shen, Z. Xu and R. Hu, *Energy & Environmental Materials*, 2020, **4**, 603-610.

22. J. Huang, X. Xie, K. Liu, S. Liang and G. Fang, *Energy & Environmental Materials*, 2022, **6**, e12309.

23. Y. Gao, J. Zhou, L. Qin, Z. Xu, Z. Liu, L. Wang, X. Cao, G. Fang and S. Liang, *Green Energy & Environment*, 2023, **8**, 1429-1436.

24. G. Liang, F. Mo, H. Li, Z. Tang, Z. Liu, D. Wang, Q. Yang, L. Ma and C. Zhi, *Advanced Energy*

Materials, 2019, **9**, 1901838.